# Validating the KAGIS black-box GIS-based model in a Mediterranean karst aquifer: case of study of Mela aquifer (SE Spain)

Javier Valdes-Abellan[a,*], Concepción Pla[a], Miguel Fernandez-Mejuto[b], José Miguel Andreu[c]

[a] *Department of Civil Engineering, University of Alicante, Alicante, Spain.*
[b] *Hydrologic Cycle, Diputación Provincial de Alicante, Spain*
[c] *Department of Earth Sciences and Environment, University of Alicante, Spain*
[*] *Corresponding author: javier.valdes@ua.es*

**ABSTRACT**

KAGIS (Karst Aquifer GIS-based) model is developed and applied to Mela aquifer, a small karst aquifer located in a Mediterranean region (SE Spain). This model considers different variables, such as precipitation, land use, surface slope and lithology, and their geographical heterogeneity to calculate both, the runoff coefficients and the fraction of precipitation which contributes to fill the soil water reservoir existing above the aquifer. Evapotranspiration uptakes deplete water, exclusively, from this soil water reservoir and aquifer recharge occurs when water in the soil reservoir exceeds the soil field capacity. The proposed model also obtains variations of the effective porosity in a vertical profile, an intrinsic consequence of the karstification processes. A new proposal from the Nash-Sutcliffe Efficiency Index, adapted to arid environments, is presented and employed to evaluate the model's ability to predict the water table oscillations. The uncertainty in the model parameters is determined by the Generalized Likelihood Uncertainty Estimation method. Afterwards, when KAGIS is calibrated, wavelet analysis is applied to the resulting data in order to evaluate the variability in the aquifer behaviour. Wavelet analysis reveals that the rapid hydrogeological response,

This article has been accepted for publication and undergone full peer review but has not been through the copyediting, typesetting, pagination and proofreading process which may lead to differences between this version and the Version of Record. Please cite this article as doi: 10.1002/hyp.13215

typical of a wide variety of karst systems, is the prevailing feature of Mela aquifer. This study proves that KAGIS is a useful tool to quantify recharge and discharge rates of karst aquifers, and can be effectively applied to develop a proper management of water resources in Mediterranean areas.

**KEYWORDS**

KAGIS, water resources, wavelet analysis, Mediterranean environments, aquifer recharge.

## 1. INTRODUCTION

Water management in the Mediterranean region is a trending topic in the research community as evidenced by the number of publications in peer-reviewed journals during last lustrum (SCOPUS reports a more-than-200-publications per year ratio that deal with "Mediterranean water resources": Moutahir et al., 2017; Sachse et al., 2017; Kourgialas et al., 2018; Marcos et al., 2018; among others). Underlying this interest is the fact that scarce water resources are a limiting factor for economic development (Molina and Melgarejo, 2016) in conjunction with numerous predictions and evidences of drastic climate change that will affect the sustainability, quantity and quality of water resources in Mediterranean areas (García-Ruiz et al., 2011). According to most climate model forecasts, an increase in temperature and a decrease in precipitation is expected at the end of the 21st century (Rey et al., 2011; Soto-García et al., 2013; IPCC, 2014). Therefore, governments and water regulators will have to deal with increasing tensions among water users. In regions where groundwater is the most important resource, water management would be more effective by using models that are capable of predicting fluctuations in water table levels and groundwater volumes (Emamgholizadeh et al., 2014).

In Alicante province (SE Spain, ~2 million inhabitants), as in other semiarid regions in the world, roughly 52 % of urban water demand is supplied from aquifers (Andreu et al., 2011). In that context, understanding the hydrodynamic behaviour of aquifers and being able to predict their behaviour through numerical groundwater modelling is essential for sustainable water resources management and for anticipating the respond to changes in extractions or climate (Scanlon et al., 2003). The appropriate management strategy would allow to quantify the recharge and discharge rates obtaining an accurate hydrogeological characterization, independently of the applied model (Gaukroger and Werner, 2011; Sedki and Ouazar, 2011; Sreekanth and Datta, 2011; Chattopadhyay et al., 2014).

However, estimation of recharge rates and water table dynamics is not an easy task due to the interaction of several factors in the process (geology, vegetation cover, topography, etc.) and, additionally, it becomes more difficult in arid and semiarid environments (Jiménez-Martínez et al., 2009). Related to arid-semiarid climates, most studies have focused on the development of techniques to provide reliable recharge estimates which consider factors such as precipitation, evapotranspiration, aquifer characteristics, geomorphological features or vegetation cover, among others (Scanlon et al., 2006). Quantifying the aquifer recharge is a challenged task that must be faced with the election of a proper methodology (Scanlon et al., 2002), and these methods also need to be adapted to local and regional geological and climatic conditions. Among the different alternatives, models with a high demand of input information may be considered more reliable. However, the uncertainty associated with both the required information to characterize the system and the input data may lead to uncertain results (Andreo et al., 2008; Hartmann et al., 2014; Kirn et al., 2017). Karst aquifers, particularly complex systems, constitute relevant water reserves worldwide (El Janyani et al., 2014) and specifically in the SE Spain. They present high heterogeneity of their carbonate system and exemplify the reliability problem associated with the input information related to aquifer characterization.

In the characterization of karst hydrogeological systems two main approaches can be considered: a distributed and a lumped approach. Distributive models allow the quantitative spatial simulation of groundwater flow (Kovács and Sauter, 2007), discretize the karst system in two- or three-dimensional grids that require the assignment of characteristic hydraulic parameters and system states (Hartmannn et al., 2014) and thus require extensive field data, both for model setup and calibration (Butscher and Huggenberger, 2008), which is not an easy task. Besides, difficulties in karst aquifers modelling exist associated to the dominance of secondary (fractures) or tertiary porosity (conduits); the hierarchical structure of

permeability; and the presence of turbulent flow (invalidating Darcy's law application) cause that this numerical model application is more problematic (Scanlon et al., 2003).

Alternatively to distributed models, global models (lumped parameter models) consider the karst aquifers as 'black or grey boxes' or systems that transform input signals into output signals (Kovacs and Sauter, 2007), based on linear or nonlinear relationships. Karst aquifers are often simulated using these lumped models (Fleury et al., 2007; Padilla and Pulido-Bosch, 2008; Martínez-Santos and Andreu, 2010) which normally reduce the required input information drastically. These models conceptualize the physical processes at the scale of the whole karst system without modelling spatial variability explicitly (Hartmann et al., 2014). The greatest advantage of lumped models application is that results obtained with them have, in many cases, the same quality than results obtained from more complex models (Martínez-Santos and Andreu, 2010).

In addition, many other analysis techniques can complement the karstic behaviour determined by models. For instance, the fact that karst systems are governed by non-stationary fluctuations assures the efficiency of wavelet analysis to quantitatively describe the influence of the different existing hydrogeological processes (Jukić and Denić-Jukić, 2011). The usefulness of wavelet analysis application to improve the understanding of karst systems has been previously demonstrated (Labat et al., 2000; Andreo et al., 2006; Tremblay et al., 2011; among others). The wavelet transform consistently defines the temporal structure of an input hydrogeological factor and its related hydrogeological consequence within a karst system.

Previous studies (Pla et al., 2016a) showed the ability of a black-box GIS-based model to predict the hydrodynamic behaviour of a karst aquifer and estimate water levels in several piezometers along the Solana aquifer in SE Spain. This previous model used different variables (land use, surface slope, lithology, precipitation, etc.) heterogeneously distributed in

the aquifer surface. The model was also characterized for calculating variable aquifer storage coefficients along the aquifer profile. The model applied in the Solana aquifer, is now named the KAGIS model (Karst Aquifer GIS-based model) after some modifications and is applied in the present study to Mela aquifer, a small non-overexploited karst aquifer located in a Mediterranean region.

The present study will be focused in determining the variations of groundwater in Mela aquifer and in the discharge flow rate of Mela spring, validating the use of KAGIS for karst aquifer simulations through the application of the model in a new and completely different conditioned carbonate aquifer. For this, KAGIS model is calibrated using a 10-year long series of piezometric levels and discharge rate data. In addition, the uncertainty in the model parameters is assessed with an equifinality study. Afterwards, a wavelet analysis is applied to establish relationships between the hydrogeological features of Mela aquifer and climatic variables to understand the response of the aquifer to the precipitation events. This topic is a key aspect to water managers in cases such as the presented, since Mela spring supplies water requirements to the nearest located village.

## 2. MATERIAL AND METHODS

### 2.1. Study area

Mela aquifer (38°42'11.7"N, 0°16'03.6"W) is located near to Confrides town (Alicante, SE Spain). The aquifer has small dimensions (0.78 $km^2$) and the entire extension constitutes the recharge area (Figure 1). Due to its relatively small size and the absence of pumping, the aquifer is a suitable natural laboratory for the study of the climatic and hydrogeological relationships under non-disturbed conditions. The aquifer is composed by Lower Cretaceous limestone with a thickness of 400 m. This material forms an anticline, which emerges and constitutes the core of the aquifer, covering the total aquifer surface. The impervious level of

Mela aquifer is defined by different levels of marls. The boundaries of the aquifer are a fault in the North and in the Southwest and an outcropping marls level in the Southeast. Most of the study area presents a strong steepness, with a slope greater than 25 %. Mediterranean scrubs (Rosmarinus officinalis, Pistacia lentiscus, Myrtus communis, Cistus albidus, Genista Scorpius, Quercus coccifera, etc.) constitute the predominant land cover in the study area. Well-developed Mediterranean forest covers approximately 19 % of the study area, and rainfed agriculture (mainly olive trees) present a few important 6.61 % of area (Figure 2). The soil is classified as loam – silty loam with little profile development ranging from 70 cm to 1 m. The aquifer recharge is accomplished entirely by the precipitation since neither irrigation returns nor lateral inlets exist in the area. Water transfer between Mela aquifer and the adjacent groundwater bodies has not been observed (DPA, 2010). Mela aquifer has a unique spring in the eastern part where the impervious marls outcrop; the spring constitutes the natural exit of the aquifer resources. From October 2005 to January 2016, Mela spring presented an average flow of 8.20 l/s. This averaged annual value varied from a minimum of 1.34 l/s to more than 16.00 l/s. The area is characterized by a Mediterranean temperate climate with dry hot summers and mild winters (Csa climate type, Köppen-Geiger Classification slightly modified (AEMET, 2011). For the studied period, mean annual temperature accounts for 14.4°C, total annual precipitation for 736 mm, and reference evapotranspiration, $ET_0$, according to FAO Penman-Monteith (Allen et al., 1998), accounts for 1075 mm.

### 2.2. Groundwater modelling

#### 2.2.1. Data acquisition

The calibration of KAGIS requires reliable real data which was obtained from various official sources. Climatic data (precipitation and temperature daily records) were provided by

AEMET (Meteorological National Agency of Spain) and were measured in the nearest existing meteorological station (38°40'24.7"N 0°12'48.7"W), around 5 km from the aquifer with no relieves between them. Daily data of piezometric level were provided by the Provincial Government of Alicante (*Diputación Provincial de Alicante*, DPA). The water table level in the aquifer is controlled by a probe installed in the unique existing well. Finally, DPA also performs regular measurements of flow rates in Mela spring gauging station, located in an open-channel. Flow rate measurements were performed with a quarterly frequency, on average, during the study period. The study period comprises 10 years (October 2005 – January 2016).

**2.2.2. Modelling Process**

KAGIS model was successfully applied in a previous study (Pla et al., 2016a) in an overexploited aquifer. The original code was adapted to the new setup and applied to Mela aquifer, whose hydrodynamic behaviour has been modelled following a structure comprised by different GIS-based information layers for land use, slope and geology properties. GIS information was obtained from the Valencian Cartographic Institute (ICV), depending on the autonomic government. Land use information defines six different classes within the aquifer boundaries. Soil slope is classified with values of: <3 %, 3–10 %, 10–15 %, 15–25 % and >25 %. The complete aquifer surface is defined by limestones (DPA, 2007) so this property is constant for the whole surface. As a result of the GIS analysis, the aquifer surface becomes divided into different polygons representing units with different hydrodynamic behaviour.

The input water in the soil-aquifer system is calculated for each individual polygon following the Spanish normative 5.2-IC (Fomento, 2016), equivalent for the SCS runoff curve numbers (Mockus, 1956). The main objective of this step is to discriminate between the fraction of precipitation that produces superficial runoff and the complementary fraction which contributes to fill the soil water reservoir.

The features of soil-epikarst placed above the aquifer directly affect the infiltration process, i.e., the transit of water from surface into the karst system responsible for the water recharge (Pardo-Igúzquiza et al., 2012). Soil properties will determine the infiltration of precipitated water to the deepest parts of the profile. The proposed model does not consider a specific component to quantify the downward flow through the karst matrix of the system, neither a transient period of water through the epikarst. However, KAGIS considers that soil water remaining after surface runoff is converted into infiltrated water going inside the soil reservoir (Figure 3); water will exit this reservoir as evapotranspiration or aquifer recharge depending on climatic conditions. KAGIS considers a depth of 1 m for the soil reservoir because this value represents the average depth of the soil profile in the study area. Thus, the infiltration mechanism is comprised through the runoff coefficient.

The runoff coefficients, $C_{i,j}$, are computed for each polygon of the aquifer area $i$ and each day of the studied period $j$ (Equation 1).

$$C_{i,j} = \begin{cases} \dfrac{\left(\dfrac{P_{i,j} \cdot K_A}{P0_i} - 1\right) + \left(\dfrac{P_{i,j} \cdot K_A}{P0_i} + 23\right)}{\left(\dfrac{P_{i,j} \cdot K_A}{P0_i} + 11\right)^2} & \text{if } P_{i,j} > P0_i \\ 0 & \text{if } P_{i,j} < P0_i \end{cases} \qquad \text{(eq. 1)}$$

where $C_{i,j}$, [-] is the fraction of the superficial component of the precipitation; $P0_i$ [mm] is the runoff initial threshold value, a constant parameter for each polygon $i$ determined in dependence on the use, slope, hydrological characteristics and texture of soil as established in 5.2-IC; $P_{i,j}$ [mm] is the input precipitation at polygon $i$ and day $j$; and $K_A$ [-] is a correcting factor dependent on the size surface, that, for this study case, is considered 1.

The runoff coefficients are affected by a model parameter, $f_1$, which multiplies all polygons of the aquifer area. In order to avoid illogical values of the final runoff coefficients (higher than 1 or lower than 0), the adaptation shown in Equation 2 is required.

The input water in soil, *IWnet* [mm], is calculated for each polygon *i* and day *j* following Equation 2:

$$IWnet_{i,j} = P_{i,j} \cdot \left[ C_{i,j} + C_{i,j} \cdot f_1 \cdot \left(1 - C_{i,j}\right) C_{i,j} \right] \quad \text{(eq. 2)}$$

where all parameters have been defined previously. With the definition shown in Equation 2, the model is able to modify the runoff coefficients given by the normative up to 25 % of its original value. Additionally, the capacity to modify the runoff coefficients is lower when the initial runoff coefficients are close to 0 or close to 1. Thus, soils that are initially very impermeable/permeable will remain in similar values.

Water not producing surface runoff enters into the soil reservoir (Figure 3). The idea of considering the soil as a water reservoir as an intermediate step before the aquifer recharge was used by Fleury et al. (2007). The soil reservoir capacity varies for each polygon of the study area since it is dependent of the field capacity, $fc_i$. This field capacity was adopted from Twarakavi et al. (2009), ranging from 0.02 to 0.35, and assigned to each polygon according to their land use.

Evapotranspiration uptake, $ET_0$, depletes water from this soil water reservoir exclusively. Evapotranspiration is produced at its potential rate when there is enough water in the soil reservoir, and eventually becomes zero when the soil reservoir is completely empty. In the present study, the FAO Penman-Monteith method (Allen et al., 1998) is employed to calculate $ET_0$ for each polygon *(i)* and with a daily periodicity. KAGIS calculates the water in the soil reservoir state for each polygon and day following Equation 3 and 4. Similar approaches to KAGIS models can be found in Martos-Rosillo et al. (2013; 2015); Allocca et al. (2015) or Kirn et al. (2017).

$$SR_{i,j} = SR_{i,j-1} + IWnet_{i,j} - ET_{0i,j} \quad \text{(eq. 3)}$$

where $SR_{i,j}$ [mm] is the value of the water in the soil reservoir volume at polygon *i* and day *j*, and $SR_{i,j-1}$ [mm] is the water in the soil reservoir volume at the same polygon *i* the previous day *j-1*.

Aquifer recharge takes place exclusively when $SR_{i,j}$ is above the maximum value of the soil water reservoir (i.e. higher than field capacity). Description of all possible situations related with aquifer recharge and the soil water reservoir is collected in Equation 4.

$$if \begin{cases} fc_i < SR_{i,j} & Re_{i,j} = SR_{i,j} - fc_i; & SR_{i,j} = fc_i \\ 0 < SR_{i,j} < fc_i & Re_{i,j} = 0; & \\ SR_{i,j} < 0 & Re_{i,j} = 0; & SR_{i,j} = 0 \end{cases} \quad \text{(eq. 4)}$$

where $Re_{i,j}$ [mm] is the recharge rate of the aquifer system at polygon *i* and day *j;* and $fc_i$ [$m^3$ $m^{-3}$] is the field capacity at polygon *i*.

This structure implies that recharge will take place mainly through soils with low field capacity (mainly limestones in the study area) since the small size of the soil reservoir allows a faster filling with low precipitation rates. Additionally, ET losses will be mainly produced in those polygons with high values of their field capacity.

The individual recharge calculated for all the different polygons is then totalized for the whole surface of the aquifer in the form of recharge volume (*Re*) by the consideration of the polygon areas. Total balance of water is calculated daily, and finally piezometric level variation ($\Delta z$) is calculated following Equation 5.

$$\Delta z_j = \frac{Re_j - f_5 \cdot SD_j}{p(z) \cdot S_{aqf}} \quad \text{(eq. 5)}$$

where $\Delta z_j$ is the water table fluctuation [m] predicted at day *j*; $Re_j$ [$m^3$] is the recharge rate of the aquifer system at day *j*; $SD_j$ is water volume daily discharged by the natural Mela spring [$m^3$] at day *j; p(z)* is the porosity value at *z* level above the sea level; and $S_{aqf}$ [$m^2$] is the total aquifer surface. In the present case, neither well extractions, irrigations returns nor lateral inlets were considered and then no information about those parameters has been included in

the equations of this study; nevertheless, the model structure in such more complex study cases would be the same as it was previously shown in Pla et al. (2016a). $f_i$ are weighting factors [-] adjusted by the Simplex search method of Lagarias et al. (1999) which minimizes the objective function value and obtains the best calibration factor values. Spring discharge was related to piezometric level by the hydraulic head (i.e. difference between the water table and the spring level) to the power of 1.5, following general expressions of hydraulic weirs.

In the present study, the objective function was defined as the sum of the differences between the observed and modelled data to the power of 4. This definition was an attempt to adapt the optimization engine to the climatic characteristics of the region. In the region, the hydrological behaviour features a high quantity of data close to minimum values and eventual short extraordinary events. With such dynamics, sum of square errors would lead to models able to predict average values but unable to predict the extraordinary events.

Calibration is made in two steps: first, all the factors, including an initial effective porosity average value, are obtained; second, effective porosity is obtained independently for each depth (discretization of 20 cm), setting the average value of porosity obtained in the first step as the initial value for the second step. Therefore, the proposed model obtains an effective porosity profile and is able to detect the presence of high porosity levels, corresponding to depths where karstification processes have been more intense, if any. The latter aspect stablishes a distinctive characteristic of the presented model since in karst aquifers the existence of conduits, cavities and caverns implies that groundwater accumulates in these preferential locations instead of in the primary rock porosity. All calculations of this stage were carried out using MATLAB R2015.a ® software.

**2.3. Goodness-of-fit assessment**

The *NRMSE* (normalised root mean square error) and the *ANSE* (Nash-Sutcliffe Efficiency index adapted for arid environments) were the statistical indicators selected to determine the ability of the model to simulate the observed values.

$$NRMSE = \frac{1}{x_{\mathrm{o,max}} - x_{\mathrm{o,min}}} \sqrt{\frac{1}{n}\sum_{i=1}^{n}\left(x_{i,\mathrm{o}} - x_{i,s}\right)^2} \qquad \text{(eq. 6)}$$

$$ANSE = 1 - \frac{\sum_{i=1}^{n}\left(x_{i,\mathrm{o}} - x_{i,\mathrm{s}}\right)^4}{\sum_{i=1}^{n}\left(x_{i,\mathrm{o}} - \overline{x_{\mathrm{o}}}\right)^4} \qquad \text{(eq. 7)}$$

where $x_{i,\mathrm{o}}$ is the observed value at time $i$; $x_{i,\mathrm{s}}$ is the simulated value at time $i$; $\overline{x_{\mathrm{o}}}$ is the mean observed value; $x_{\mathrm{o,max}}$ is the maximum observed value; and $x_{\mathrm{o,min}}$ is the minimum observed value. For *NRMSE*, the optimal value is zero, indicative of a perfect fit between estimated and observed values, while threshold values of 0.2-0.3 are considered acceptable (Wallis et al., 2011). Normalization of the *RMSE* is a required process to facilitate the comparison between datasets or models with different scales. The *NSE* index is a widely used statistic to assess the predictive power of hydrological models (Nash and Sutcliffe, 1970). In the Nash-Sutcliffe Efficiency Index, *NSE* equals to 1 for a perfect fit; *NSE* is equal to 0, when predicted values are as accurate as the mean of the observations; and *NSE* below 0 indicates that model predictions are worse than the mean of observations. In the present study, an adaptation of the *NSE* for arid environments, the *ANSE*, is presented. With such hydrodynamic behaviour, the standard *NSE* index overweighs average values so a new proposal was used. The unique modification is the value of the differences exponent, from 2 in the standard definition to 4, so more importance is given to extreme values. Other values of the exponent as 6 or 8 were also checked but results using these exponents did not change significantly to the use of 4, so the new definition was kept as close as possible to the original NSE. As in the standard *NSE*

index, the *ANSE* ranges from [1,-∞[, corresponding 1 to the perfect fit and zero to the model whose performance is as good as the average observed value.

### 2.4. Uncertainty assessment

The GLUE (Generalized Likelihood Uncertainty Estimation) method (Beven and Binley, 1992) was employed to assess the uncertainty in the model parameters, its uniqueness and the uncertainty in water table predicted values. The GLUE method is based in Monte Carlo simulations which flexibly define the likelihood function and its boundary value employed to distinguish between behavioural and non-behavioural solutions. The uncertainty analysis is a required step when dealing with high-parameter models because the solution existence domain increases exponentially with the number of parameters. The first step consisted in defining randomly chosen sets of all parameters involved in the study; uniform distribution function between logical boundaries was adopted as the engine to obtain the random values. Then a number of runs were carried out with those parameter sets, and the likelihood function was obtained for all runs. In this study we used the EF index, defined above, as the likelihood function following previous studies as the Beven and Binley (1992) or Mannina et al. (2010) with a threshold value of 0.15. The non-behavioural runs were rejected, and the weights of the rest were re-scaled. With the re-scaled sets, probability distribution functions were obtained for each parameter with the predictive uncertainty predictions associated with the 5 % and the 95 %.

### 2.5. Wavelet analysis

The discharged water volume in Mela spring and the precipitation follow a nonstationary behaviour, a particular feature of the hydrological signals. In this study, the relationship between the hydrogeological and climatic features in Mela aquifer is unveiled

using the wavelet analysis. With this analysis, the nonstationary signals are located both in time and frequency domain, and thus the detection of changes in the evaluated signals is easily accomplished with the aim of establishing the frequency domain where precipitation mostly influences the karst system behaviour. Wavelet analyses a signal at different time-frequency resolutions through scaled and translated versions of a mother wavelet. For this study case, based in previous studies with satisfactory results (Pla et al., 2016b) Daubechies is the selected mother wavelet. The wavelet analysis and filtering of Mela signals is developed with the Environmental Wavelet Tool (Galiana-Merino et al., 2014), a MATLAB-based code designed to examine environmental time series. Although some briefly descriptions about wavelet theory are provided below, extended aspects of wavelet analysis may be consulted (e.g.: Daubechies, 1992; Kaiser, 1994; Wickerhauser, 1994; Strang and Nguyen, 1996).

In the continuous wavelet transform (CWT), the wavelet function works as a band-pass filter well located in frequency and time. Consequently, the CWT results correspond to the analysis (or filtering) of the signal at some specific selected time-period ranges (scales). Mela behaviour is evaluated by implementing cross wavelet transform (XWT) and wavelet transform coherence (WTC) between two CWTs, so as to determine relationships between two signals in the time domain and to recognize common behaviours between calculated discharged flow and precipitation records.

While XWT provides interrelations between two time-domain signals, WTC analyses the coherence and phase lag between two time series as a function of both, time and frequency. XWT checks the wavelet power with a significance test at every point in the time/scale plane. As a consequence, the analysis between pairs of signals results in the identification of areas with high common power in XWT and WTC. In this study, a

MATLAB software package developed by Grinsted et al. (2004) is employed to implement XWT and WTC.

Discrete wavelet transform (DWT) performs a multiresolution analysis of signals following a sub-band coding scheme (Mallat, 1989) supported on two quadrature filters (based on the respective mother wavelet) that work as high-pass and low-pass filters plus downsampling by a factor of 2. These filters are successively applied for each scale or level of the wavelet decomposition providing two new signals (the detail and approximation coefficients, each one associated with a theoretical period band).

Multiresolution cross-analysis (Labat et al., 2002; Charlier et al., 2015) quantifies relationship between two signals across scales. The cross-correlation function gives a measure of the similarity of variations over time between two time series (Proakis and Manolakis, 1988). In practice, the normalized cross-correlation function provides a value between -1 and 1; the higher the similarity of variations over time, the higher the correlation coefficient.

## 3. RESULTS AND DISCUSSION

### 3.1. Modelled results

Results from GIS analysis divide the aquifer surface into 22 polygons with different characteristics. GIS analysis confirmed that nearly 90 % of the aquifer surface presents a slope greater than 25 % covered mostly by Mediterranean scrubs and forests.

The 100 % of the surface is dominated by material with medium permeability as defined by the qualitative permeability classification established by (DPA, 2003; DPA, 2010). This classification, and according to the different existing land uses, relates to a moderate infiltration capacity in agreement to the 5.2-IC normative. As a result, the

calculated runoff initial threshold values, $P0_i$, vary from 21 to 47 mm depending on the different polygons.

Observed and simulated values of water table levels are depicted in Figure 4a and observed and simulated water discharges in Mela spring are depicted in Figure 4b. Precipitation events are also represented, showing the main characteristics of Mediterranean climate with long periods of unimportant precipitation events and eventual very important precipitation forced by atmospheric convective processes. The minimum piezometric level detected during the monitored period was 731.33 masl (i.e. meters above sea level), coincident with Mela spring level. Aquifer response to precipitation events are observed shortly after the events, highlighting the small impact that the soil water reservoir (see section 2.2.2) has in the study area, which is in agreement with the significant area occupied by limestone outcrops. After the important increment in piezometric levels, water table stabilizes slower to its base level where it normally remains until the new precipitation event. It is worthy to notice that different stabilization levels were observed along the monitored period; this fact is completely unexpected since the stabilization level should be the same and could be explained by human errors during the installation of the probe used to monitored the piezometric level. Those differences in the stabilization level were below 30 cm in the study period. Mela spring acted in a similar way to the piezometric level, with very small flowrates during the vast majority of time (tens of litres/second), even dry during some periods and eventual very important events as a response of the aquifer discharge process.

Piezometric levels obtained by KAGIS reported good agreement between the observed and simulated values. Similar trustworthy results were also obtained in the simulation of the karst groundwater levels in previous studies (e.g., Adinehvand et al., 2017; Brenner et al., 2018). In the present study, main differences between the observed and simulated values

were identified between September 2009 and September 2011, probably related to the abovementioned problems in the measurement of the experimental values.

These results were obtained with a value of 0.08 for the $f_1$ weighting factor, affecting the runoff coefficient and a value of 0.8 for the $f_5$ weighting factor, which affects the spring discharge values. Those values highlight that the runoff coefficient was reduced an 8 % by KAGIS and that the registered values in the Mela spring have required to be reduced a 20 % according to KAGIS.

With regard to porosity and its variation along the aquifer profile, results reported an average value of 1.8 % with very small variations along the complete profile. KAGIS detected only small increments of porosity around 731 masl and so it can be considered that variation in this parameter in Mela aquifer is not important and there are no depths with different hydrodynamic behaviours. These values match with the characteristic value of pore volume in karst aquifers as it has been shown in other studies (Bauer et al., 2016; Różkowski and Różkowski, 2016).

Parameters affecting irrigation returns, lateral inlets or well extractions were setup to zero during the modelling process. However, as the model pretends to be applicable in a wide range of different karst aquifers, these factors may appear in the general equation if they were required. Results of the fitting: *ANSE* equals to 0.89 and *NRMSE* equals to 0.06 indicate that the model responds satisfactorily and performs a reliable simulation of the temporal evolution of water table depths and water volume discharge of the aquifer.

A last analysis, developed with the GLUE methodology established the uncertainty in the obtained solution. More than three thousand rounds were required to get two thousand behavioural combinations of parameters. Considered boundaries to obtain uniform random combinations were [-1, 1] for the $f_1$ weighting factor affecting the runoff coefficient; [0, 5] for the $f_5$ factor affecting the spring discharge and [0, 0.1] for the average value of porosity.

Scatter plots in Figure 5 refer to the performance of each trial, which was assessed by the use of the ANSE index. Figure 5 only collects results from the behavioural combinations, as stated previously. With regard to weighting parameters $f_5$ and average porosity (codified as $f_6$ in Figure 5), the most significant set of parameters corresponded to values in agreement with the parameters obtained with the calibration process. In case of the weighting parameter $f_1$ there was not a clear trend. An almost horizontal pattern in the significance level highlighted the small impact of parameter $f_1$ to the objective index (i.e. ANSE). Therefore, the Simplex search method employed in this study was able to get a solution close to the global minimum of the problem.

### 3.2. Variability of the aquifer behaviour: wavelet analysis applied to KAGIS results.

KAGIS simulation allowed to obtain the variations of piezometric levels in Mela aquifer and the water discharge in Mela spring for the study period. When using these results with a deeper complementary evaluation (accomplished by the wavelet analysis) it is possible to determine and understand the aquifer response to climatic occurrences.

Usually, there is a rise in the peak flow in Mela spring in response to heavy rainfall. As an example, the highest daily rainfall is registered in October 2007 (183 mm) and, consequently, a day after also occurs the highest instantaneous flow (556 l/s) in response to a substantial increase in the water table depth (Figure 4). The promptly response of Mela spring to precipitated water confirms the high transmissivity of the infiltration zone of the system.

KAGIS does not consider temporal variability in the karst system. Temporal variability in karst aquifers, both in flow dynamics (Li et al., 2014; Pacheco Castro et al., 2018) and/or in water quality (Hartmann et al., 2012; Ravbar, 2013; Delbart et al., 2014), occurs in response to different hydrologic and climatic conditions, which may result in changes in flow directions and velocities and may have an impact on karst springs. In the present study case,

KAGIS simulated fairly well the aquifer dynamics. Small temporal variations in aquifer conditions, as a consequence of the inherent characteristic of Mediterranean climate in the region, with very long dry periods and very short rainfall events, may explain the small temporal variations in aquifer conditions. Temporal variations have been observed more frequently in climates with higher rainfall rates and clearer seasonal patterns.

The seasonal behaviour of the aquifer establishes two annual periods of maximum activity in Mela spring. The maximum flows usually occur in spring and autumn, although variations in the discharge rates are totally related to rainfall amount (Figure 4b). In winter and summer seasons, Mela karst system presents a lower hydrodynamic response with low groundwater variations due to the scarce precipitations. Thus, changes in the climatic features (mostly in the precipitation regime) directly affect to the increase of Mela water table depth and, consequently, to the discharge of Mela spring.

Humid and dry periods and changes in the spring discharge are identified with the studied time series (precipitation, piezometric level and discharged water) expressed as deviation from the mean (Figure 6). Maximum annual precipitation is identified in 2007. A constant decreasing trend in rainfall through years establishes that 2014 is the driest year with a total annual amount of 334 mm. In response to this, water table variations and Mela discharges also decrease from the beginning to the end of the registered data. The lowest volume of discharged water is registered, consecutively, in 2014 and 2015 with an average instantaneous discharge of 1.3 and 3.0 l/s respectively. Calculated annual volume discharges varied from 0.51 $hm^3$ in 2007 to 0.04 $hm^3$ in 2014. In 2015, in response to rainfall, Mela aquifer discharges 0.09 $hm^3$.

The multiresolution cross-correlation performed with precipitation (as input signal) and discharged volume (as output signal) helps to confirm the frequency domain where precipitation mostly influences the karst system behaviour. The cross-correlation function is

developed between the overall input precipitation (non-decomposed time series) and an isolated output signal of discharged water at different multiresolution levels (Charlier et al., 2015), after filtering the original signal using Daubechies as mother wavelet. The different multiresolution levels vary from 1 to 1024 days (Figure 7). The highest correlation (0.41) occurs for level 1, corresponding to 1-day resolution period. Correlation of 0.19 defines level 2, corresponding to 4-8 days resolution. This correlation confirms that the studied times series (precipitation and Mela spring discharge) mainly co-vary in the high frequency domain (i.e. daily variations), which supports the nearly instantaneous response of Mela spring to heavy rainfall. In addition, correlation also peaks in level 6 (0.18), related to the discharge occurred at scale with lower frequency (64-128 days) as consequence of the seasonal distribution of rainfalls. Cumulative rainfall distributed in several days (autumn precipitation occurred in 2007, 2008, 2009 and 2012) generates continuous water floods from the soil reservoir to the aquifer that imprint Mela discharge at seasonal scale.

To identify relationships between precipitation and Mela discharge in the multi-annual frequency domain, XWT (Figure 8a) and WTC (Figure 8b) are calculated between two CWTs. The WTC stablishes local correlation between the time series in all the evaluated time frequency space. Despite this high coherence, just the unveiled areas with high common power in XWT are confirmed by the areas of locally phase locked behaviour in WTC (Grinsted et al., 2004). Connection between the two time series is confirmed by the phase-arrows pointing right in both, XWT and WTC.

The XWT analysis (Figure 8a) exhibits large common spectral power regions in the time-frequency domain within the annual (365-day) band, with phase-related signals. This band only exists from 2006 to 2013. The variation in the large-scale rainfall distribution is consequence of changes in the precipitation regime. In the driest periods (2014 and 2015 present the minimum total annual precipitation), the 365-day band of high power disappears

as Mela spring reduces the activity. Thus, annual periodicity in discharge rate is detected just in the humid years. A 10 to 8-year component is also observed from 2008 to 2013 coincident with those years with the lowest mean deviations, with annual total precipitation close to 750 mm. The seasonal response (also detected in Figure 7) is highlighted by the frequency band of 64-128 days, existent in 2008-2010 and 2013.

For all the study period (2005 to 2015), regions with large common spectral power in XWT analysis prevail in the high-frequency band (1-32 days), pointing to the rapid response of Mela spring to precipitations. The daily periodicity is always existent, also confirmed by the highest correlation detected in Figure 7. Rainfall and discharge are mostly correlated in the high frequency domain, related to the rapid hydrogeological reaction of Mela aquifer to rainfall events.

Hydrogeological response to climatic variations presents three principal kinds of components: a constant daily component, typical of highly karstified aquifers, a seasonal component, existent in the periods with strongly marked seasonality (abundant rainfalls in spring and autumn) and an annual component, visible in the most humid years. The later component is not detected in the last period of the studied time series as consequence of the decreasing trend presented by precipitation regime in the study area.

These statements demonstrate that aquifer recharge, the main water resource in the studied region and mostly concentrated in several days, is directly affected by the reduction in the number of very wet days. Particularly, in the eastern Mediterranean coast of the Iberian Peninsula it has been recently demonstrated (Valdes-Abellan et al., 2017) that average of total annual precipitation decreased by up to 15 % in the last three decades with a decrease in the number of wet days above 1 mm and in the frequency of heavy precipitation events. Future occurrences, with general tendency for annual-mean conditions to be warmer and drier

at the aquifer surface location, will lead to a very concerning scenario that water managers must consider to accomplish with all the water needs.

## 4. CONCLUSIONS

In many Mediterranean areas the water scarcity inhibits, in part, the economic growth. Consequently, the estimation and quantification of the recharge rates in the aquifers is essential to ensure the global development of these regions. With this study, we demonstrate the usefulness of employing black-box models, and particularly, the KAGIS model tool to evaluate the hydrodynamic behaviour of karst aquifers. These aquifers are very complex and heterogeneous mediums for which the application of simple models, as the one presented in this study, is an effective alternative to the standard models that have higher requirements of input information.

KAGIS has proved to obtain good results with heterogeneous karst systems through the use of weighting factors that modify the most prominent sources of unreliability, such as, the infiltration or runoff coefficient, the porosity of the aquifer and, if required, the spring discharge. KAGIS is able to deal with more complex schemes including well extractions, lateral inlets or irrigation returns to the aquifer.

The case study in the present work offered the possibility to validate the KAGIS model in Mela aquifer. The relation between the discharge rates and the piezometric levels was solved through the general expression of hydraulic weirs. Wavelet analysis applied to the data resulting from KAGIS confirmed the existing high correlation between rainfall and discharged water volume in Mela spring, pointing to the rapid hydrogeological response of the karst system.

This study also presents a new proposal for a statistical index: the Nash-Sutcliffe Efficiency index adapted for arid environments (*ANSE*), which provides an innovative contribution to the study of Hydrology in arid/semiarid environments.

In order to improve and better demonstrate the KAGIS model robustness, next step should be to apply it to different aquifers with different size, hydrogeological characteristics and heterogeneity. Even though, the application of the proposed method, combining KAGIS results with wavelet analysis, has been proved to be an efficient method to understand the behaviour of karst aquifers. KAGIS could be a solution to deal with lack of information in observed data, which would no longer suppose a problem to water managers. In addition, wavelet analysis permits detection of changes in nonstationary signals and thus, this analysis allows quantifying the most significant frequency domains where climatic variables influence the hydrological variables. Future work will be focused in developing prediction tools to determine the effect of climate change in underground water table depths in Mediterranean karst aquifers, an interesting topic of great importance in the present.

**ACKNOWLEDGEMENTS**

This research was funded by the Spanish Ministry of Science and Innovation, projects CGL2013-48802-C3-3-R and CGL2015-69773-C2-1-P; and by the University of Alicante, projects GRE15-19 and GRE17-12. Gratitude is also expressed to the Government of the Alicante Province (Diputación de Alicante) who provided the original data.

## REFERENCES


Adinehvand R, Raeisi E, Hartmann A. 2017. A step-wise semi-distributed simulation approach to characterize a karst aquifer and to support dam construction in a data-scarce environment. J. Hydrol., 554: 470-481. DOI: 10.1016/j.jhydrol.2017.08.056.

AEMET, Spanish Agency of Meteorology. 2011. Iberian Climate Atlas. Air temperature and precipitation (1971-2000) AEMET, Agencia Estatal de Meteorologia.

Allen RG, Pereira LS, Raes D, Martin S. 1998. Crop evapotranspiration - Guidelines for computing crop water requirements - FAO Irrigation and drainage paper 56. Food and Agriculture Organization of the United Nations.

Allocca V, De Vita P, Manna F, Nimmo JR. 2015. Groundwater recharge assessment at local and episodic scale in a soil mantled perched karst aquifer in southern Italy. J. Hydrol., **529**: 843-853. DOI: 10.1016/j.jhydrol.2015.08.032.

Andreo B, Jiménez P, Durán JJ, Carrasco F, Vadillo I, Mangin A. 2006. Climatic and hydrological variations during the last 117-166 years in the south of the Iberian Peninsula, from spectral and correlation analyses and continuous wavelet analyses. J. Hydrol., **324**: 24-39. DOI: 10.1016/j.jhydrol.2005.09.010.

Andreo B, Vías J, Durán JJ, Jiménez P, López-Geta JA, Carrasco F. 2008. Methodology for groundwater recharge assessment in carbonate aquifers: Application to pilot sites in southern Spain. Hydrogeol. J., **16**: 911-925. DOI: 10.1007/s10040-008-0274-5.

Andreu JM, Alcalá FJ, Vallejos Á, Pulido-Bosch A. 2011. Recharge to mountainous carbonated aquifers in SE Spain: Different approaches and new challenges. J. Arid Environ., **75**: 1262-1270. DOI: 10.1016/j.jaridenv.2011.01.011.

Bauer H, Schröckenfuchs TC, Decker K. 2016. Hydrogeological properties of fault zones in a karstified carbonate aquifer (Northern Calcareous Alps, Austria). Hydrogeol. J., **24**: 1147-1170. DOI: 10.1007/s10040-016-1388-9.

Beven K, Binley A. 1992. The future of distributed models: model calibration and uncertainty prediction. Hydrol. Processes, **6**: 279-298.

Brenner S, Coxon G, Howden NJK, Freer J, Hartmann A. 2018. Process-based modelling to evaluate simulated groundwater levels and frequencies in a Chalk catchment in south-western England. Nat. Hazards Earth Syst. Sci., 18: 445-461. DOI: 10.5194/nhess-18-445-2018.

Butscher C, Huggenberger P. 2008. Intrinsic vulnerability assessment in karst areas: A numerical modeling approach. Water Resources Research, **44**. DOI: 10.1029/2007WR006277.

Charlier JB, Ladouche B, Maréchal JC. 2015. Identifying the impact of climate and anthropic pressures on karst aquifers using wavelet analysis. J. Hydrol., **523**: 610-623. DOI: 10.1016/j.jhydrol.2015.02.003.

Chattopadhyay PB, Vedanti N, Singh VS. 2014. A Conceptual Numerical Model to Simulate Aquifer Parameters. Water Resources Management, **29**: 771-784. DOI: 10.1007/s11269-014-0841-6.

Daubechies I. 1992. Ten lectures on wavelets. SIAM. DOI: 10.1137/1.9781611970104.

Delbart C, Valdes D, Barbecot F, Tognelli A, Richon P, Couchoux L. 2014. Temporal variability of karst aquifer response time established by the sliding-windows cross-correlation method. J. Hydrol., **511**: 580-588. DOI: 10.1016/j.jhydrol.2014.02.008.

DPA Diputación Provincial de Alicante. 2003. Mapa Hidrogeológico Provincial de Alicante. Memoria. Diputación de Alicante.

DPA Diputación Provincial de Alicante. 2007. Mapa del Agua, Provincia de Alicante. Diputación de Alicante.

DPA Diputación Provincial de Alicante. 2010. Mapa Hidrogeológico, Provincia de Alicante. Diputación de Alicante.

El Janyani S, Dupont JP, Massei N, Slimani S, Dörfliger N. 2014. Hydrological role of karst in the Chalk aquifer of Upper Normandy, France. Hydrogeol. J., **22**: 663-677.

Emamgholizadeh S, Moslemi K, Karami G. 2014. Prediction the Groundwater Level of Bastam Plain (Iran) by Artificial Neural Network (ANN) and Adaptive Neuro-Fuzzy Inference System (ANFIS). Water Resources Management, **28**: 5433-5446. DOI: 10.1007/s11269-014-0810-0.

Fleury P, Plagnes V, Bakalowicz M. 2007. Modelling of the functioning of karst aquifers with a reservoir model: Application to Fontaine de Vaucluse (South of France). J. Hydrol., **345**: 38-49.

Fomento Md. 2016. Norma 5.2 - IC drenaje superficial de la Instrucción de Carreteras.

Galiana-Merino JJ, Pla C, Fernandez-Cortes A, Cuezva S, Ortiz J, Benavente D. 2014. EnvironmentalWaveletTool: Continuous and discrete wavelet analysis and filtering for environmental time series. Comput Phys Commun, **185**: 2758-2770. DOI: 10.1016/j.cpc.2014.06.011.

García-Ruiz JM, López-Moreno JI, Vicente-Serrano SM, Lasanta-Martínez T, Beguería S. 2011. Mediterranean water resources in a global change scenario. Earth Sci. Rev., **105**: 121-139. DOI: 10.1016/j.earscirev.2011.01.006.

Gaukroger AM, Werner AD. 2011. On the Panday and Huyakorn surface-subsurface hydrology test case: Analysis of internal flow dynamics. Hydrol. Processes, **25**: 2085-2093. DOI: 10.1002/hyp.7959.

Grinsted A, Moore JC, Jevrejeva S. 2004. Application of the cross wavelet transform and wavelet coherence to geophysical times series. Nonlinear Processes Geophys., **11**: 561-566. DOI: 10.1029/2003JD003417.

Hartmann A, Lange J, Weiler M, Arbel Y, Greenbaum N. 2012. A new approach to model the spatial and temporal variability of recharge to karst aquifers. Hydrol. Earth Syst. Sci., **16**: 2219-2231. DOI: 10.5194/hess-16-2219-2012.

Hartmann A, Mudarra M, Andreo B, Marín A, Wagener T, Lange J. 2014. Modeling spatiotemporal impacts of hydroclimatic extremes on groundwater recharge at a mediterranean karst aquifer. Water Resources Research, **50**: 6507-6521. DOI: 10.1002/2014WR015685.

Hartmann A, Goldscheider N, Wagener T, Lange J, Weiler M. 2014. Karst water resources in a changing world: Review of hydrological modeling approaches. Rev. Geophys., **52**: 218-242. DOI: 10.1002/2013RG000443.

IPCC TIPoCC. 2014. Climate Change 2014: Synthesis Report.

Hartmann A, Mudarra M, Andreo B, Marín A, Wagener T, Lange J. 2014. Modeling spatiotemporal impacts of hydroclimatic extremes on groundwater recharge at a mediterranean karst aquifer. Water Resources Research, **50**: 6507-6521. DOI: 10.1002/2014WR015685.

Jiménez-Martínez J, Skaggs TH, van Genuchten MT, Candela L. 2009. A root zone modelling approach to estimating groundwater recharge from irrigated areas. J. Hydrol., **367**: 138-149.

Jukić D, Denić-Jukić V. 2011. Partial spectral analysis of hydrological time series. J. Hydrol., **400**: 223-233. DOI: 10.1016/j.jhydrol.2011.01.044.

Kaiser G. 1994. A Friendly Guide to Wavelets. Springer Science+Business Media.

Kirn L, Mudarra M, Marín A, Andreo B, Hartmann A. 2017. Improved Assessment of Groundwater Recharge in a Mediterranean Karst Region: Andalusia, Spain. In: EuroKarst 2016, Neuchâtel, Renard P, Bertrand C (eds.) Springer International Publishing, pp: 117-125.

Kourgialas NN, Karatzas GP, Dokou Z, Kokorogiannis A. 2018. Groundwater footprint methodology as policy tool for balancing water needs (agriculture & tourism) in water scarce islands - The case of Crete, Greece. Sci. Total Environ., **615**: 381-389. DOI: 10.1016/j.scitotenv.2017.09.308.

Kovács A, Sauter M. 2007. Modelling karst hydrodynamics. In: Karst Hydrogeology, Goldscheider N, Drew D (eds.) Taylor and Francis, pp: 201-222.

Labat D, Ababou R, Mangin A. 2000. Rainfall-runoff relations for karstic springs. Part II: Continuous wavelet and discrete orthogonal multiresolution analyses. J. Hydrol., **238**: 149-178. DOI: 10.1016/S0022-1694(00)00322-X.

Labat D, Ababou R, Mangin A. 2002. Multiresolution cross-analysis of rainfall rates and karstic spring runoffs. C. R. Geosci., **334**: 551-556. DOI: 10.1016/S1631-0713(02)01795-9.

Lagarias JC, Reeds JA, Wright MH, Wright PE. 1999. Convergence properties of the Nelder-Mead simplex method in low dimensions. SIAM Journal on Optimization, **9**: 112-147.

Li X, Wang YQ, Liu LH. 2014. The spatial-temporal variability of karst water chemistry in houzhai karst basin, Guizhou, China. Wu X, Chen W, Yang W, Liang J (eds.) Trans Tech Publications Ltd, pp: 114-118.

Mallat SG. 1989. A Theory for Multiresolution Signal Decomposition: The Wavelet Representation. IEEE Trans Pattern Anal Mach Intell, **11**: 674-693. DOI: 10.1109/34.192463.

Mannina G, Di Bella G, Viviani G. 2010. Uncertainty assessment of a membrane bioreactor model using the GLUE methodology. Biochem. Eng. J., **52**: 263-275. DOI: 10.1016/j.bej.2010.09.001.

Marcos R, Llasat MC, Quintana-Seguí P, Turco M. 2018. Use of bias correction techniques to improve seasonal forecasts for reservoirs — A case-study in northwestern Mediterranean. Sci. Total Environ., **610-611**: 64-74. DOI: 10.1016/j.scitotenv.2017.08.010.

Martínez-Santos P, Andreu JM. 2010. Lumped and distributed approaches to model natural recharge in semiarid karst aquifers. J. Hydrol., **388**: 389-398.

Martos-Rosillo S, González-Ramón A, Jiménez-Gavilán P, Andreo B, Durán JJ, Mancera E. 2015. Review on groundwater recharge in carbonate aquifers from SW Mediterranean (Betic Cordillera, S Spain). Environ. Earth Sci., **74**: 7571-7581. DOI: 10.1007/s12665-015-4673-3.

Martos-Rosillo S, Rodríguez-Rodríguez M, Pedrera A, Cruz-SanJulián JJ, Rubio JC. 2013. Groundwater recharge in semi-arid carbonate aquifers under intensive use: The Estepa Range aquifers (Seville, southern Spain). Environ. Earth Sci., **70**: 2453-2468. DOI: 10.1007/s12665-013-2288-0.

Mockus V. 1956. Hydrology Guide for Use in Watershed Planning. Soil Conservation Service, U.S. Department of Agriculture.

Molina A, Melgarejo J. 2016. Water policy in Spain: seeking a balance between transfers, desalination and wastewater reuse. Int. J. Water Resour. Dev., **32**: 781-798. DOI: 10.1080/07900627.2015.1077103.

Moutahir H, Bellot P, Monjo R, Bellot J, Garcia M, Touhami I. 2017. Likely effects of climate change on groundwater availability in a Mediterranean region of Southeastern Spain. Hydrol. Processes, **31**: 161-176. DOI: 10.1002/hyp.10988.

Nash JE, Sutcliffe JV. 1970. River flow forecasting through conceptual models part I — A discussion of principles. J. Hydrol., **10**: 282-290.

Pacheco Castro R, Pacheco Ávila J, Ye M, Cabrera Sansores A. 2018. Groundwater Quality: Analysis of Its Temporal and Spatial Variability in a Karst Aquifer. Groundwater, **56**: 62-72. DOI: 10.1111/gwat.12546.

Padilla A, Pulido-Bosch A. 2008. Simple procedure to simulate karstic aquifers. Hydrol. Processes, **22**: 1876-1884. DOI: 10.1002/hyp.6772.

Pardo-Igúzquiza E, Durán-Valsero JJ, Dowd PA, Guardiola-Albert C, Liñan-Baena C, Robledo-Ardila PA. 2012. Estimation of spatio-temporal recharge of aquifers in mountainous karst terrains: Application to Sierra de las Nieves (Spain). J. Hydrol., 470-471: 124-137. DOI: 10.1016/j.jhydrol.2012.08.042.

Pla C, Valdes-Abellan J, Tenza-Abril AJ, Benavente D. 2016a. Predicting Daily Water Table Fluctuations in Karstic Aquifers from GIS-Based Modelling, Climatic Settings and Extraction Wells. Water Resources Management: 1-15. DOI: 10.1007/s11269-016-1302-1.

Pla C, Galiana-Merino JJ, Cuezva S, Fernandez-Cortes A, Cañaveras JC, Benavente D. 2016b. Assessment of CO2 dynamics in subsurface atmospheres using the wavelet approach: from cavity–atmosphere exchange to anthropogenic impacts in Rull cave (Vall d'Ebo, Spain). Environ. Earth Sci., **75**. DOI: 10.1007/s12665-016-5325-y.

Proakis JG, Manolakis DG. 1988. Introduction to Digital Signal Processing. Macmillan.

Ravbar N. 2013. Variability of groundwater flow and transport processes in karst under different hydrologic conditions. Acta Carsologica, **42**: 327-338.

Rey D, Garrido A, Mínguez MI, Ruiz-Ramos M. 2011. Impact of climate change on maize's water needs, yields and profitability under various water prices in Spain. Span. J. Agric. Res., **9**: 1047-1058.

Romanazzi A, Gentile F, Polemio M. 2015. Modelling and management of a Mediterranean karstic coastal aquifer under the effects of seawater intrusion and climate change. Environ. Earth Sci., **74**: 115-128. DOI: 10.1007/s12665-015-4423-6.

Różkowski J, Różkowski K. 2016. Influence of fissuring and karstification of the carbonate aquifer unsaturated zone on its vulnerability to contamination (Cracow Upper Jurassic Region, Poland). Environ. Earth Sci., **75**. DOI: 10.1007/s12665-016-5790-3.

Scanlon BR, Healy RW, Cook PG. 2002. Choosing appropriate techniques for quantifying groundwater recharge. Hydrogeol. J., **10**: 18-39.

Scanlon BR, Keese KE, Flint AL, Flint LE, Gaye CB, Edmunds WM, Simmers I. 2006. Global synthesis of groundwater recharge in semiarid and arid regions. Hydrol. Processes, **20**: 3335-3370. DOI: 10.1002/hyp.6335.

Scanlon BR, Mace RE, Barrett ME, Smith B. 2003. Can we simulate regional groundwater flow in a karst system using equivalent porous media models? Case study, Barton Springs Edwards aquifer, USA. J. Hydrol., **276**: 137-158.

Sedki A, Ouazar D. 2011. Simulation-Optimization Modeling for Sustainable Groundwater Development: A Moroccan Coastal Aquifer Case Study. Water Resources Management, **25**: 2855-2875. DOI: 10.1007/s11269-011-9843-9.

Sachse A, Fischer C, Laronne JB, Hennig H, Marei A, Kolditz O, Rödiger T. 2017. Water balance estimation under the challenge of data scarcity in a hyperarid to Mediterranean region. Hydrol. Processes, **31**: 2395-2411. DOI: 10.1002/hyp.11189.

Soto-García M, Martínez-Alvarez V, García-Bastida PA, Alcon F, Martin-Gorriz B. 2013. Effect of water scarcity and modernisation on the performance of irrigation districts in south-eastern Spain. Agric. Water Manage., 124: 11-19.

Sreekanth J, Datta B. 2011. Coupled simulation-optimization model for coastal aquifer management using genetic programming-based ensemble surrogate models and multiple-realization optimization. Water Resources Research, 47. DOI: 10.1029/2010WR009683.

Strang G, Nguyen T. 1996. Wavelets and Filter Banks. Wellesley-Cambridge Press.

Tremblay L, Larocque M, Anctil F, Rivard C. 2011. Teleconnections and interannual variability in Canadian groundwater levels. J. Hydrol., 410: 178-188. DOI: 10.1016/j.jhydrol.2011.09.013.

Twarakavi NKC, Šimůnek J, Schaap MG. 2009. Development of Pedotransfer Functions for Estimation of Soil Hydraulic Parameters using Support Vector Machines Soil Sci. Soc. Am. J., **73**: 1443-1452. DOI: 10.2136/sssaj2008.0021.

Valdes-Abellan J, Pardo MA, Tenza-Abril AJ. 2017. Observed precipitation trend changes in the western Mediterranean region. Int. J. Climatol. DOI: 10.1002/joc.4984.

Wallis KJ, Candela L, Mateos RM, Tamoh K. 2011. Simulation of nitrate leaching under potato crops in a Mediterranean area. Influence of frost prevention irrigation on nitrogen transport. Agric. Water Manage., **98**: 1629-1640.

Wickerhauser MV. 1994. Adapted Wavelet Analysis: From Theory to Software. Taylor & Francis.

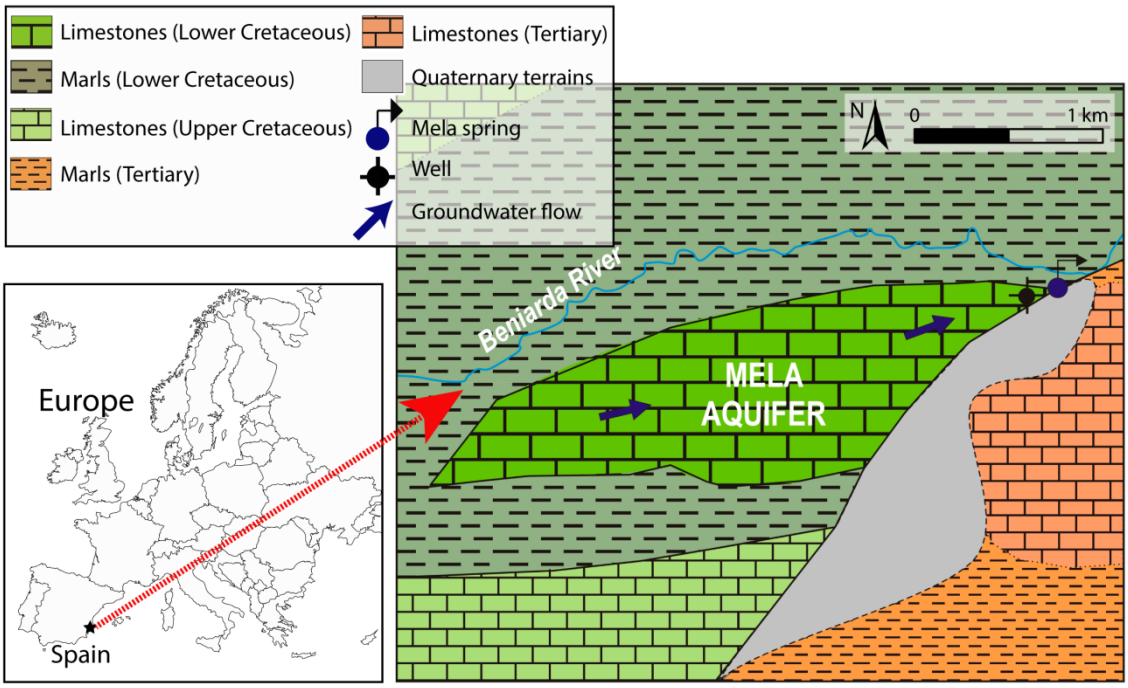


Figure 1. Geographical location and geological scheme of the study area.

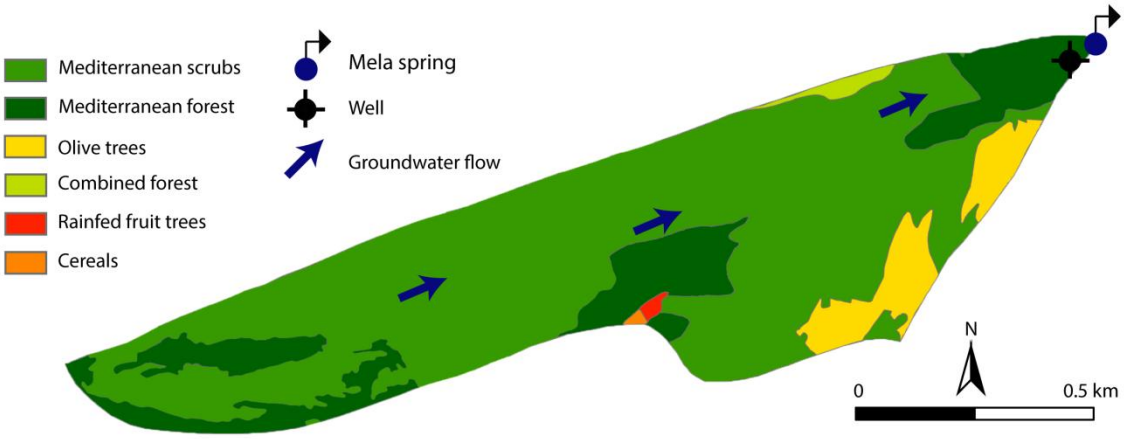


Figure 2. Land use map.

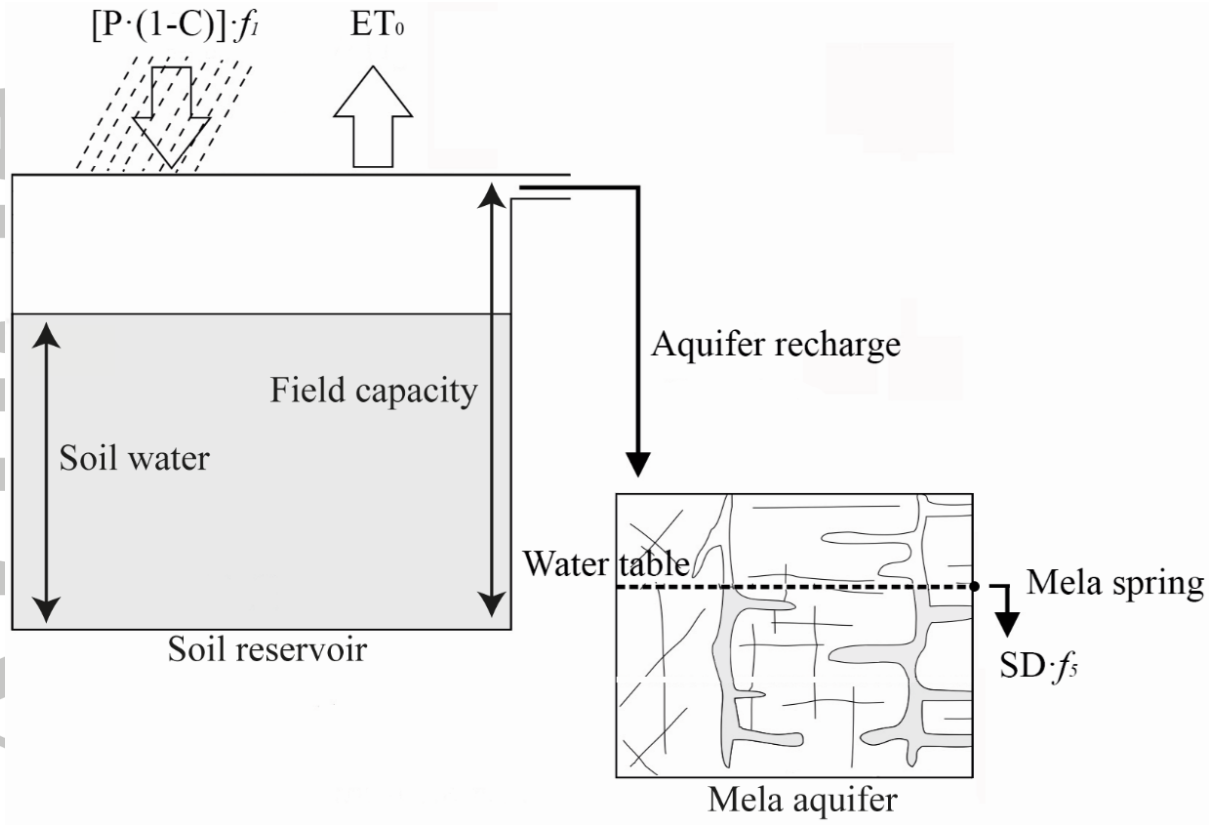


Figure 3. Soil reservoir and Mela recharge model scheme.

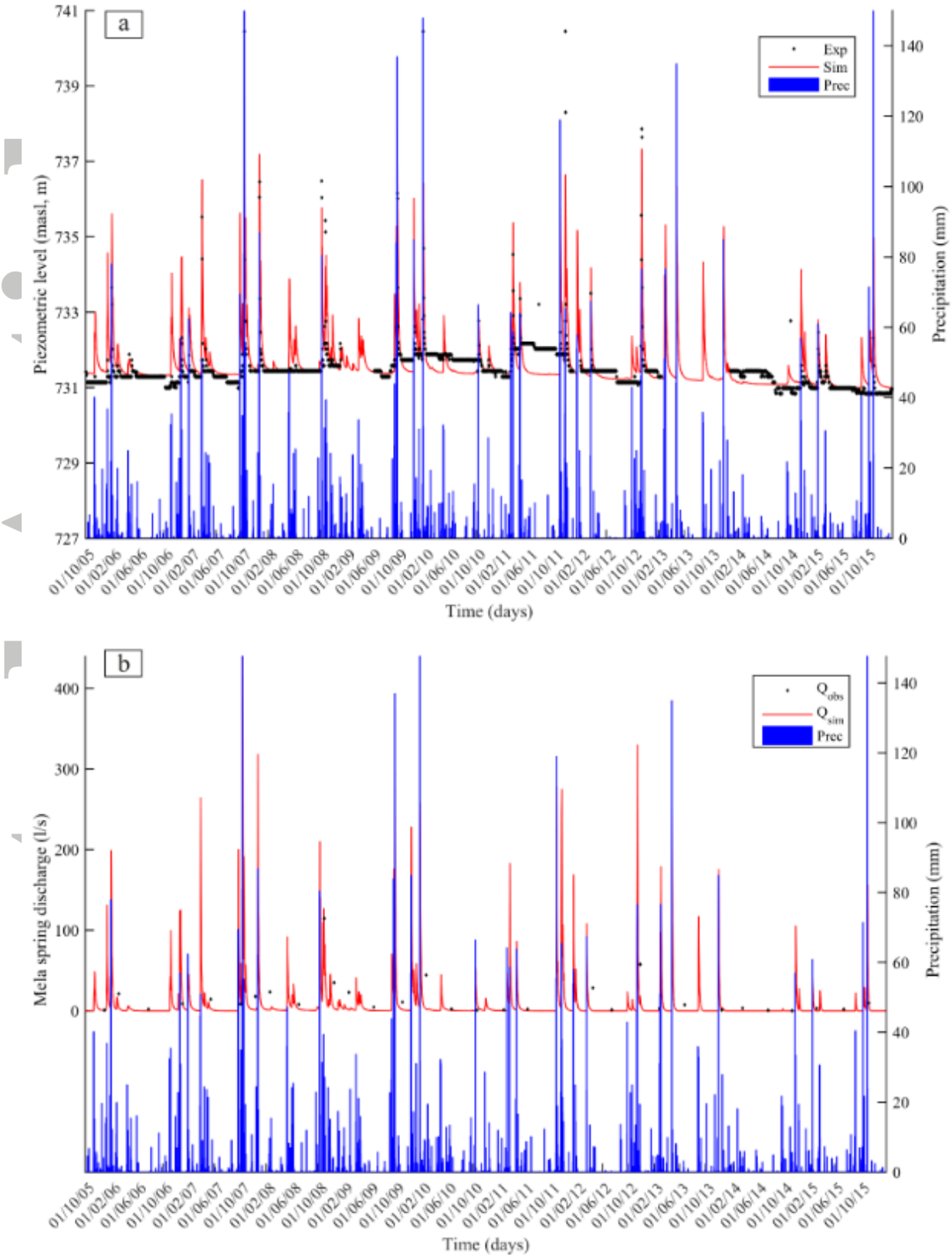


Figure 4. Observed (black dots) and simulated (red line) piezometric levels (part a), spring water discharge (part b), and precipitation (blue bars) for the observed period.

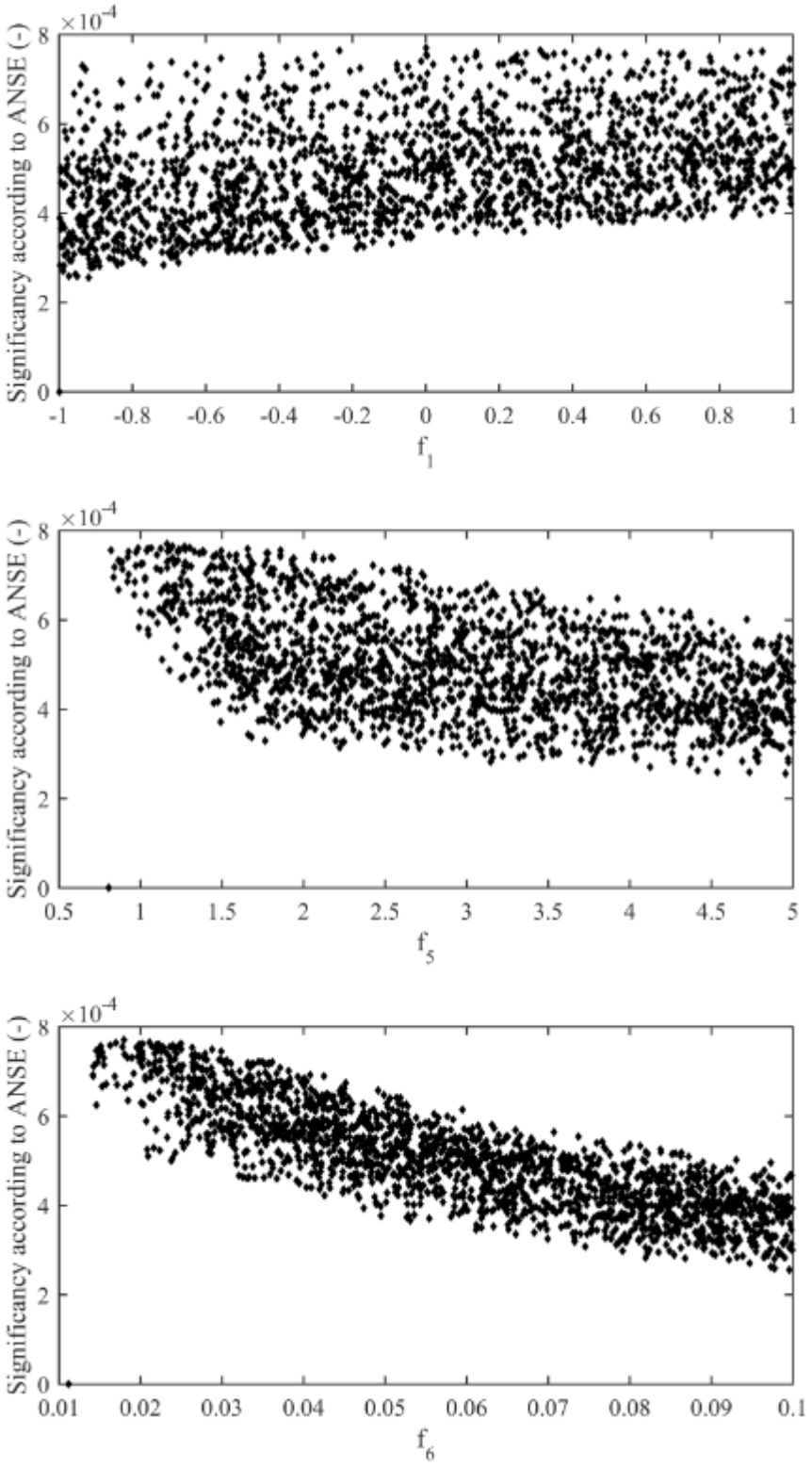


Figure 5. Significant scatter plots of the weighting parameters according to ANSE

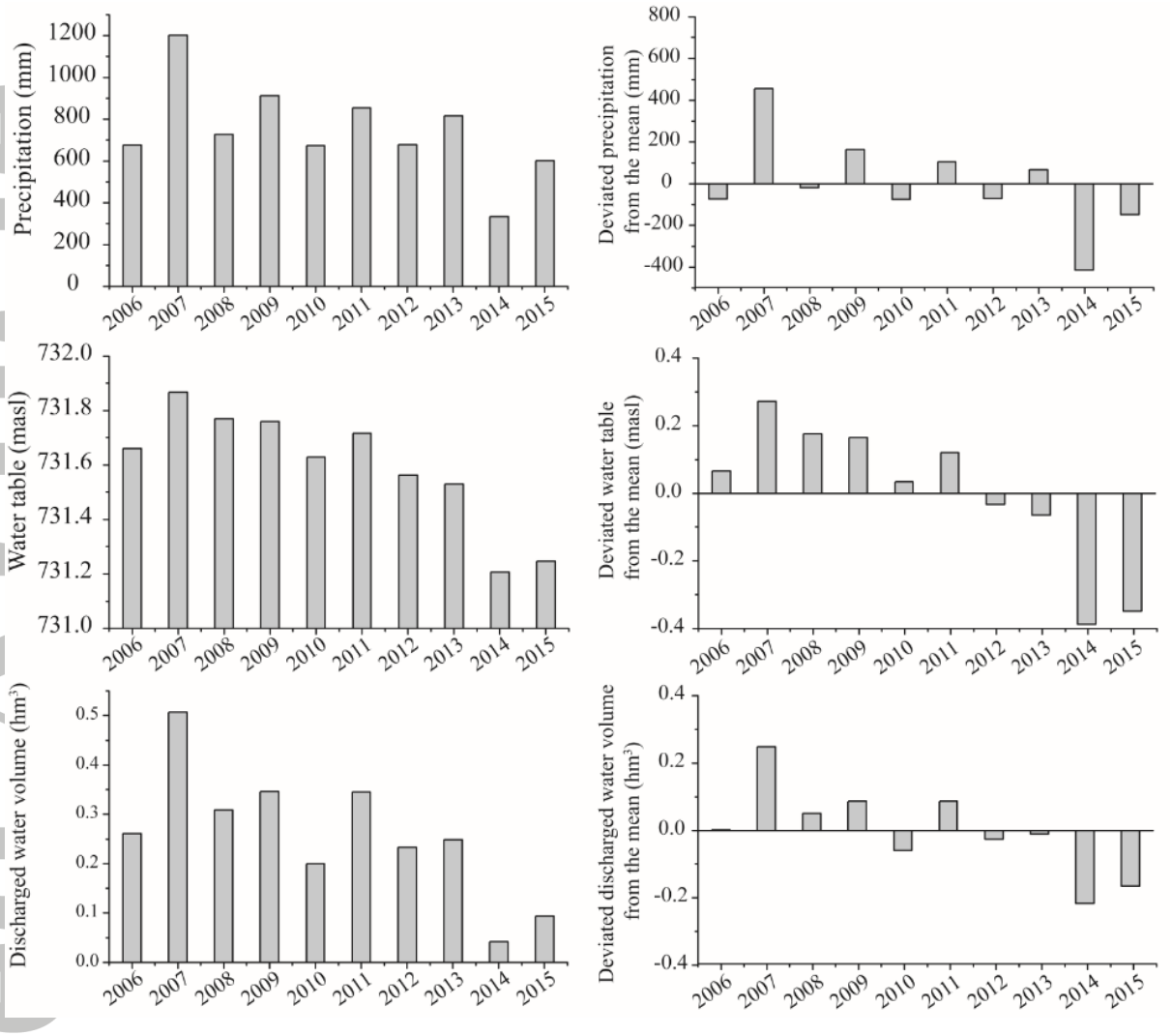


Figure 6. Annual precipitation (mm), average water level (masl) and accumulated annual discharged volume ($hm^3$) and deviated values from the mean.

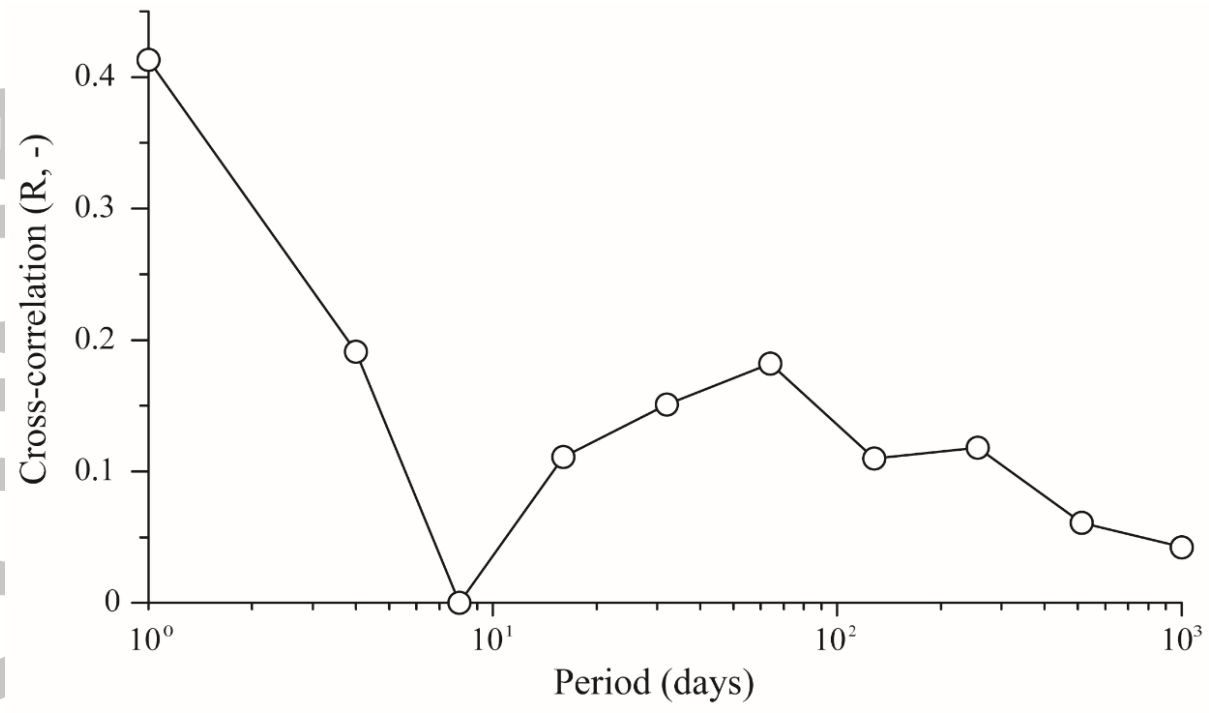


Figure 7. Cross-correlation function between overall precipitation (input signal) and discharged water at different multiresolution levels (output signal).

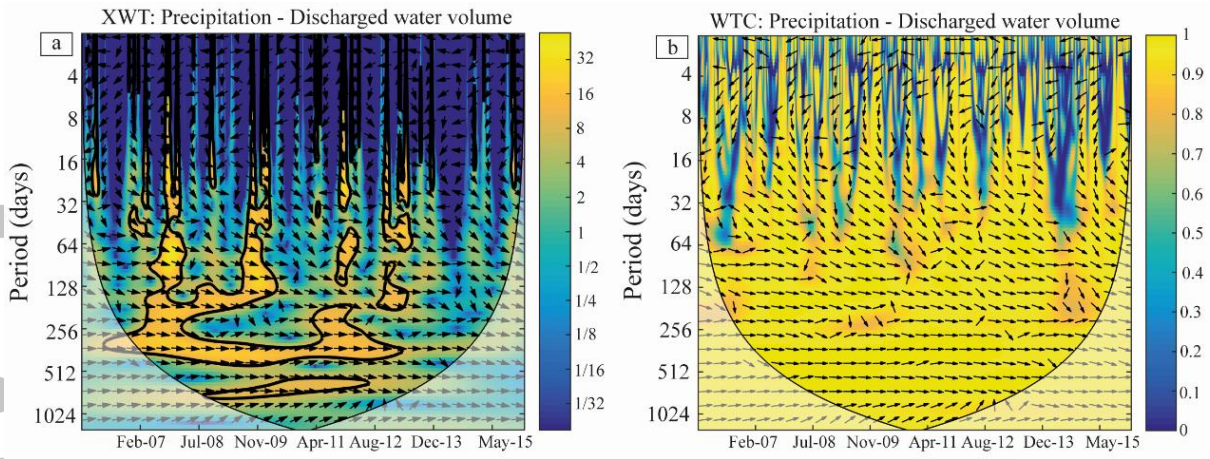


Figure 8. XWT (a) and WTC (b) between precipitation and Mela discharge in the multi-annual frequency domain. Spectral strength and coherence range from dark (weak) to light (strong) colours. Arrows indicate the relative phase relationship (in-phase pointing right, anti-phase pointing left, one signal leading the other by 90º pointing up/down). Curved lines indicate the cone of influence where edge effects become important.